Action potential propagation in mitral cell lateral dendrites is decremental and controls recurrent and lateral inhibition in the mammalian olfactory bulb

Troy W. Margrie*, Bert Sakmann, and Nathaniel N. Urban

Abteilung Zellphysiologie, Max-Planck-Institut für Medizinische Forschung, Jahnstrasse 29, D-69120 Heidelberg, Germany

Contributed by Bert Sakmann, November 2, 2000

In the mammalian main olfactory bulb (MOB), the release of glutamate from lateral dendrites of mitral cells onto the dendrites of granule cells evokes recurrent and lateral inhibition of mitral cell activity. Whole-cell voltage recordings in the mouse MOB *in vivo* and *in vitro* show that recurrent and lateral inhibition together control the number, duration, and onset of odor-evoked action potential (AP) firing in mitral cells. APs in mitral cells propagate into the lateral dendrites and evoke a transient increase in dendritic calcium concentration ($[Ca^{2+}]$), which is decremental with distance from the soma, and increases with AP number. These results suggest that the extent of AP propagation in lateral dendrites of mitral cells, along with the concomitant dendritic Ca^{2+} transient, controls the amplitude of lateral and recurrent inhibition and thus is a critical determinant of odor-specific AP patterns in the MOB.

In the mammalian olfactory system, olfactory-receptor neuron (ORN) activity is transformed by the neuronal circuitry of the main olfactory bulb (MOB) into odor-specific action potential (AP) patterns. ORNs are broadly tuned and increase their activity monotonically with increasing odorant concentration (1, 2). In contrast, odor-evoked responses in mitral/tufted (M/T) cells, the principal cells of the MOB, often are more specific and show both increases and decreases in AP firing rate with increasing concentrations of odorant (3). This transformation of the ORN activity into M/T cell activity within the MOB depends on recurrent and lateral inhibition (4).

ORN axons terminate in the glomeruli of the MOB, where they provide the only source of extrinsic excitatory input to M/T cells. APs in M/T cells result in release of glutamate from their lateral dendrites, evoking γ-aminobutyric acid (GABA)-ergic recurrent and lateral inhibition via dendrodendritic synapses with granule cells (5–11). Recurrent and lateral inhibition of M/T cells are thought to be important in odor discrimination (12) and also in the generation and synchronization of odor-evoked rhythmic mitral cell activity (13, 14).

The mechanisms by which recurrent inhibitory postsynaptic potentials (IPSPs) regulate subthreshold and suprathreshold odor-evoked M/T cell activity have not been examined directly (4, 12, 15, 16). Although recent *in vitro* studies have elucidated the mechanisms underlying transmitter release at dendrodendritic synapses, the functional role of dendrodendritic inhibition *in vivo* remains unclear (17–20). In particular, the relationship between the firing rate of a mitral cell and the strength of recurrent inhibition evoked is not known.

M/T cell lateral dendrites spread across large regions of the MOB (21), suggesting that granule cell-mediated lateral inhibition is important also for the patterning of activity across wide regions of the MOB. Propagation of APs into M/T cell dendrites is thought to be required for evoking glutamate release (17–20) onto granule cell dendrites. Thus, the propagation of APs in mitral cell lateral dendrites could determine the spatial extent of lateral inhibition evoked by M/T cell firing. In the apical dendrites of mitral cells, APs back-propagate without decrement (22, 23). Here we examine AP propagation in lateral dendrites of mitral cells to determine the conditions under which widespread lateral and recurrent inhibition is activated.

We show that odor-evoked recurrent inhibition causes accommodation of AP firing, and odor-evoked lateral inhibition can prevent AP firing of mitral cells that receive active ORN input. The *in vivo* recordings allowed us to determine the amplitude and activity-dependence of the isolated recurrent IPSP evoked by a single mitral cell under physiological conditions. Single and dual whole-cell voltage recordings combined with dendritic calcium imaging *in vitro* showed that propagation of APs differs between the apical and the lateral mitral cell dendrites, and in lateral dendrites the spatial spread of activation is decremental and increases with AP activity. The results are consistent with the view that odor-evoked AP firing causes a rise in dendritic $[Ca^{2+}]_i$ thus determining the strength of recurrent and lateral inhibition.

Materials and Methods

***In Vivo* and *in Vitro* Electrophysiology.** Horizontal olfactory bulb slices (300 μm thick) were prepared from anesthetized mice and rats (Ketamine 0.1%/Xylazine 0.1%; P18-P40) and maintained in Ringer's solution containing (in mM): NaCl 125, KCl 2.5, $NaHCO_3$ 25, NaH_2PO_4 1.25, $MgCl_2$ 1, glucose 25, and $CaCl_2$ 2. *In vivo* experiments were carried out on freely breathing mice (P21-P35) anesthetized with urethane (1.2 g/kg, i.p.). Access to the olfactory bulb was gained via a hole drilled through the cranium 1 mm anterior to the rhinal fissure and 0.75 mm lateral to the midline. A custom-built chamber was sealed to the cranium to enable superperfusion of solutions (37°C). A custom-built olfactometer (24) was used to present odors to the nares. After the experiments, the brains were fixed, coronally sectioned (250–300 μm), and processed (25) to reveal cell morphology (Fig. 1*A*). Because of some surface damage from repeated electrode penetrations, the apical tufts of mitral cells sometimes were not recovered. All animal care was performed in accordance with the guidelines of the Max Planck Society.

For both *in vitro* and *in vivo* recordings, patch pipettes (3–6 MΩ, 8–15 MΩ for dendritic recordings) were pulled from borosilicate glass tubing and filled with solutions containing (in mM): potassium-gluconate 130, Hepes 10, $MgCl_2$ 2, MgATP 2,

Abbreviations: ORN, olfactory-receptor neuron; MOB, main olfactory bulb; AP, action potential; M/T, mitral/tufted; IPSP, inhibitory postsynaptic potential; AA, amyl acetate; GABA, γ-aminobutyric acid.

*To whom reprint requests should be addressed. E-mail: tmargrie@sun0.mpimf-heidelberg.mpg.de.

The publication costs of this article were defrayed in part by page charge payment. This article must therefore be hereby marked "*advertisement*" in accordance with 18 U.S.C. §1734 solely to indicate this fact.

Article published online before print: *Proc. Natl. Acad. Sci. USA*, 10.1073/pnas.011523098. Article and publication date are at www.pnas.org/cgi/doi/10.1073/pnas.011523098

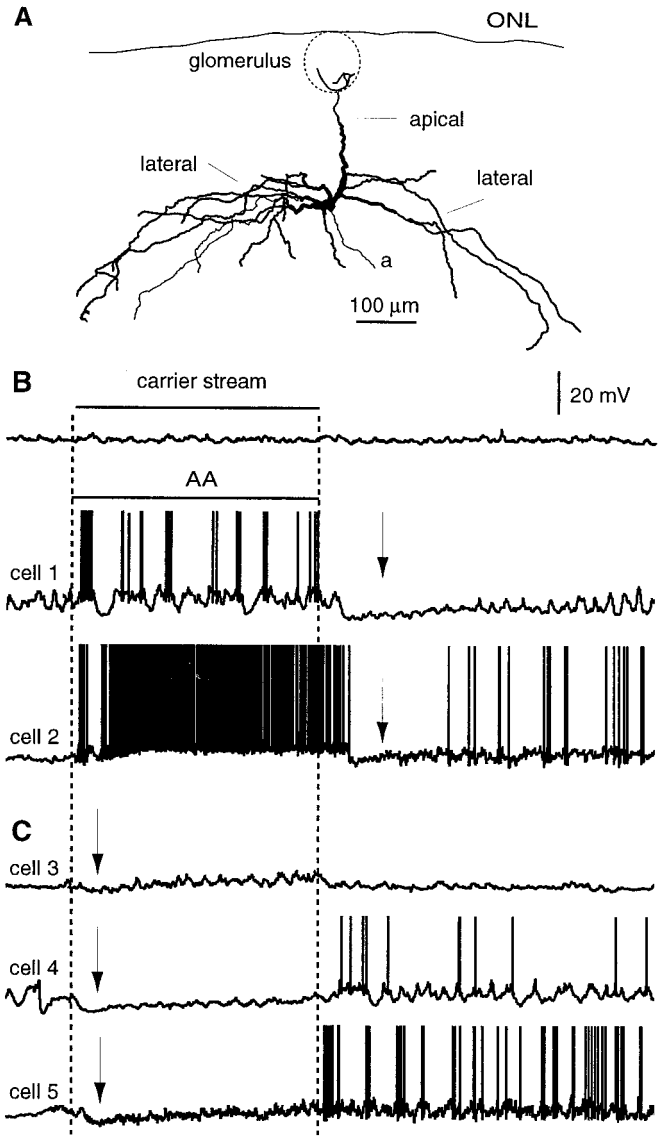

Fig. 1. Odor-evoked responses in mitral cells. (*A*) Projection of the reconstruction of the morphology of a mitral cell recorded *in vivo* with apical and lateral dendrites. The outline of a glomerulus is shown schematically. (*B*) Examples of odor-evoked excitatory responses. AA but not the carrier stream (cell 1) evokes APs (up to 250 s^{-1}) in mitral cells (APs are clipped). Moderate or high odor-evoked firing rates result in abrupt decreases in firing rates and hyperpolarizations (arrows) following termination of the odor presentation. (*C*) Examples of odor-evoked hyperpolarizations (arrows). AA under control conditions caused an initial hyperpolarization, followed by a transient burst of spikes after termination of the stimulus. Odor presentations are 5 s.

Na_2ATP 2, GTP 0.3, NaCl 4, and biocytin 1–4%, at pH 7.3. *In vitro* whole-cell recordings were obtained by using standard techniques (26). All data have been corrected for a +7 mV junction potential. Because of the small diameter of the lateral dendrites in mice, dendritic recordings were carried out on mitral cells in rat olfactory bulb slices. Otherwise, all experiments were carried out on mice. To obtain whole-cell recordings *in vivo*, we used conventional voltage clamp methods (27). Electrodes were advanced into the brain in 2- to 3-μm steps while repeatedly applying voltage steps (6–10 mV, 10 ms duration). Positive pressure (25–50 millibars) was applied to the pipette while it was being advanced. When electrode resistance increased, the positive pressure was removed and, with slight negative pressure, a seal resistance of 1 GΩ or greater was achieved. The whole-cell configuration was achieved by applying a slow ramp of negative pressure. *In vivo*, mitral cells were identified by their distance from the surface (180–250 μm), input resistance (<160 MΩ), resting membrane potential (−51 to −62 mV), and the appearance of a recurrent IPSP following APs. *In vivo* and *in vitro* voltage recordings were amplified with the Axoclamp-2B amplifier in bridge mode (Axon Instruments, Foster City, CA), filtered at 3–10 kHz, and digitized at 5–20 kHz (ITC-16; Instrutech, Mineola, NY) with custom software running under IGOR (WaveMetrics, Lake Oswego, OR) or PULSE (HEKA Electronics, Lambrecht/Pfalz, Germany). Series resistances were from 10–70 MΩ (*in vivo*), 5–25 MΩ (*in vitro* somatic), and 15–50 MΩ (*in vitro* dendritic).

Ca^{2+} Fluorescence Imaging. Neurons were filled via the recording pipette with either 50–200 μM fura-2 or 50–100 μM calcium orange (Molecular Probes). Fluorescence was imaged with ×60 and ×20 objectives (Olympus, Hamburg) and a fixed-stage microscope (Zeiss). A monochromatic light source was used for fluorescence excitation (TILL Photonics, Planegg, Germany), and images [full frames and regions of interest (ROI)] were acquired by a back-illuminated frame-transfer charge-coupled device camera (Princeton Instruments, Trenton, NJ). When imaging fura-2 fluorescence, Ca^{2+} concentrations were calculated by using the standard ratioing equations (28, 29). Data acquisition rates ranged from 10 ms per point for ROI to 67 ms per point for full-frame images. Agents used were 2,3-dihydroxy-6-nitro-7-sulfamoylbenzo[*f*]quinoxaline (NBQX), 6-cyano-7-nitroquinoxaline-2,3-dione (CNQX), D-2-amino-5-phosphonovaleric acid (APV), bicuculline, biocytin, *n*-amyl acetate (AA) (stock: 50 or 100% diluted in mineral oil; Sigma). All data are reported as mean ± SEM.

Results

Odor-Evoked Recurrent Inhibition. Odor-evoked AP firing was examined by using *in vivo* whole-cell recordings from mitral cells (Fig. 1*A*). Odor-evoked responses fell into two general categories (30), with one fraction of cells showing increases in AP rate (Fig. 1*B*, cells 1 and 2) and other cells showing inhibition by hyperpolarization (Fig. 1*C*, cells 3–5).

The first type of odor-evoked mitral cell response was characterized by stimulus-locked AP rates up to 250 s^{-1} (Fig. 1*B*, cell 2). Mitral cells firing at high rates at the onset of odor presentation often showed a decrease in AP frequency during the stimulus and a hyperpolarization following its termination (Fig. 1*B*, cells 1 and 2, arrows). We hypothesized that both the decrease in AP rate during stimulus presentation and the after-stimulus hyperpolarization were caused by odor-evoked recurrent IPSPs. To test this view more directly, we examined the pharmacological properties of the odor-evoked IPSP and current injection-evoked IPSPs (i.e., the isolated recurrent IPSP).

Odor-evoked AP patterns were modulated by bicuculline. Fig. 2*Ai* shows an odor-evoked response that exhibited a prominent hyperpolarization (≈5 mV) after termination of the odor exposure. Superfusion of bicuculline over the MOB reduced the odor-evoked hyperpolarization, resulting in APs that outlasted the odor stimulus (Fig. 2*Ai*). Bicuculline also abolished the increase in interspike-interval (ISI) that was observed during odor presentation. Under control conditions, the ISI of odor-evoked responses increased ≈2-fold ($n = 3$) from 77 ± 7 ms (first 15 APs after burst) to 128 ± 16 ms (last 15 APs; Fig. 2*B*). In bicuculline, the ISI was unchanged during the odor response [49 ± 4 ms (first 15 APs after burst) vs. 39 ± 5 ms (last 15 APs); Fig. 2*B*].

Depolarizing current injection (100- to 150-ms steps) resulted in trains of APs that were followed by a prolonged hyperpolarization (Fig. 2*Aii*) comparable to recurrent IPSPs as described

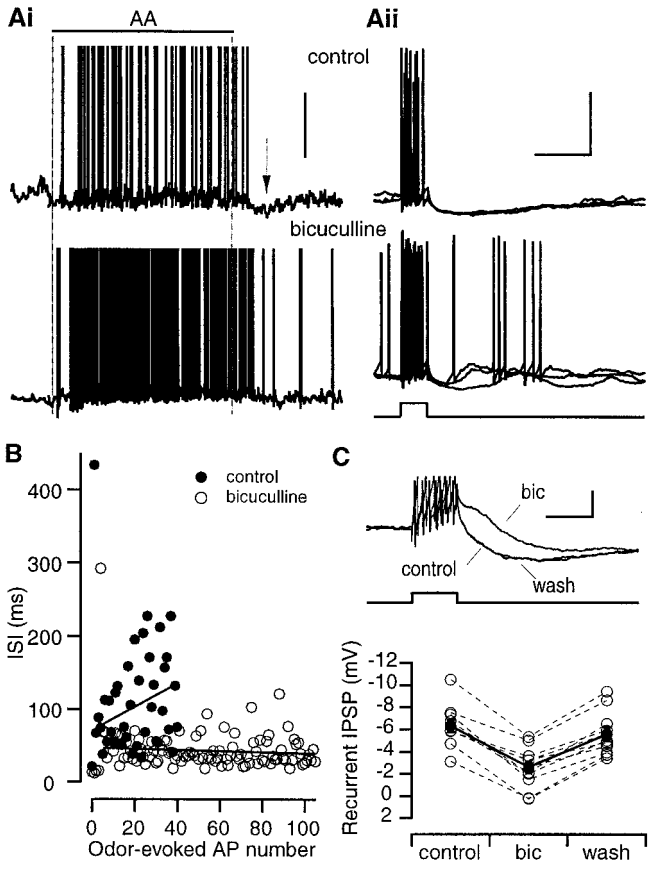

Fig. 2. Odor-evoked excitatory responses and recurrent inhibition in mitral cells. (*Ai*) AA application results in a strong odor-evoked response that is followed by a hyperpolarization. After superfusion of bicuculline, the response to AA is increased, and the hyperpolarization is eliminated. Odor presentation is 5 s, and the vertical scale bar is 20 mV. (*Aii*) Three superimposed traces show the current-evoked recurrent IPSP in the same cell as in *Ai* under control conditions and after superfusion with bicuculline. (Scale bar represents 200 ms and 40 mV.) (*B*) Interspike interval (ISI) for the odor-evoked responses shown in *A* plotted against the AP number. Lines indicate the best linear fit. (*C*) (*Upper*) Bicuculline (100 μM) superfused over the olfactory bulb (10 min) reduces the amplitude of the AP-evoked hyperpolarization in a mitral cell *in vivo*. (Scale bar represents 100 ms and 5 mV.) (*Lower*) Data from 11 cells (*in vivo*) show the reduction of the recurrent IPSP amplitude by bicuculline.

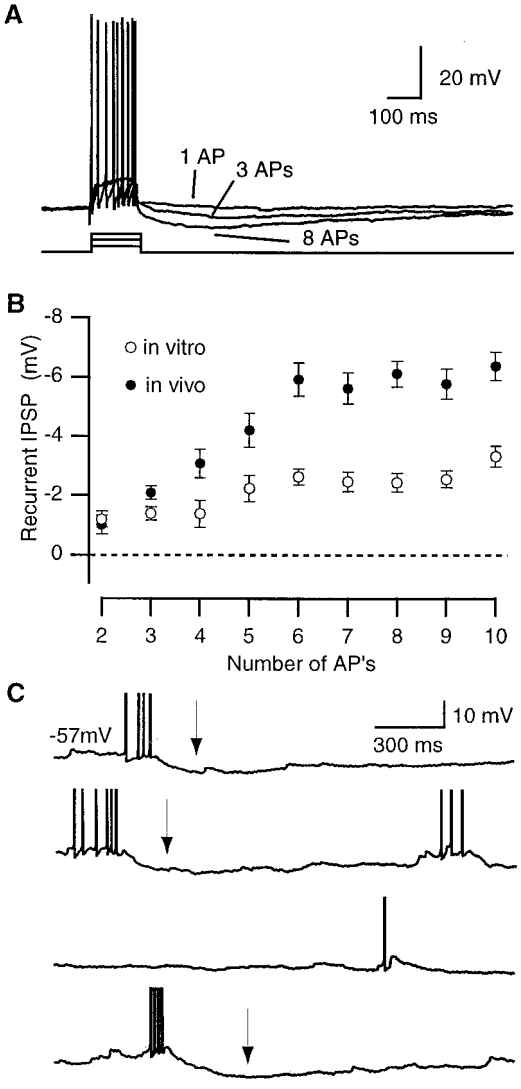

Fig. 3. AP-frequency dependence of recurrent IPSPs in mitral cells *in vivo*. (*A*) Single traces show recurrent IPSPs after APs elicited by 150-ms steps of positive current injection (120 pA, 150 pA, and 200 pA). (*B*) The peak amplitude of the recurrent IPSP increases with the number of APs evoked *in vivo* and *in vitro* (n = 17 cells *in vivo*, n = 30 cells *in vitro*). (*C*) AP-associated hyperpolarizations were observed in mitral cells *in vivo* after spontaneous bursts of two or more APs but usually not after a single AP (APs are clipped).

(10, 11, 17, 18, 31) *in vitro* (decay time constant: 459 ± 87 ms, n = 13). This hyperpolarization was blocked also by bicuculline (5.7 ± 0.6 mV vs. 2.2 ± 0.4 mV control and bicuculline, respectively; n = 11, $P < 0.001$; Fig. 2*C*), indicating that it represents the isolated, recurrent IPSP.

Therefore, the recurrent IPSP shapes odor-evoked mitral cell AP patterns in two ways. First, during prolonged odor presentation, the IPSP reduces the rate of mitral cell firing. Secondly, after the cessation of a sensory input, the hyperpolarization caused by the recurrent IPSP rapidly and precisely terminates mitral cell firing.

Mechanisms of Recurrent Inhibition. The *in vivo* experiments suggest that the amplitude of the recurrent IPSP depends on the rate of mitral cell firing. Consistent with this idea, when isolated recurrent IPSPs were elicited by bursts of APs evoked by somatic current injection, the amplitude of the IPSP depended on the number of APs in the burst [−3.1 ± 0.5 mV (4 AP), −6.4 ± 0.5 mV (10 AP), n = 17; Fig. 3 *A* and *B*], suggesting that APs at higher than 10 APs s^{-1} effectively evoke recurrent IPSPs. A similar dependence of recurrent-IPSP amplitude on AP number was observed *in vitro* [−1.4 ± 0.4 mV (4 AP), −3.3 ± 0.3 mV (10 AP), n = 30; $P < 0.001$; Fig. 3*B*], although the amplitude of the recurrent IPSP *in vitro* was reduced. *In vivo*, bursts of spontaneously generated APs, but usually not single APs, also produced prolonged hyperpolarizations (Fig. 3*C*). Thus, odor-evoked, current-evoked, and spontaneous recurrent IPSPs *in vivo* increased with AP frequency. The difference in the recurrent IPSP amplitude between the *in vivo* and *in vitro* preparations may reflect the elimination of inhibitory synaptic connections during the slicing procedure or a difference in the ionic concentrations in the extracellular milieu and suggest that *in vitro* experiments underestimate the contribution of the recurrent IPSP *in vivo*.

Because sampling of natural odors occurs over many seconds, for dendrodendritic inhibition to contribute to odor processing, it must remain effective during long periods of mitral cell activity. Therefore, we next evoked mitral cell activity for periods

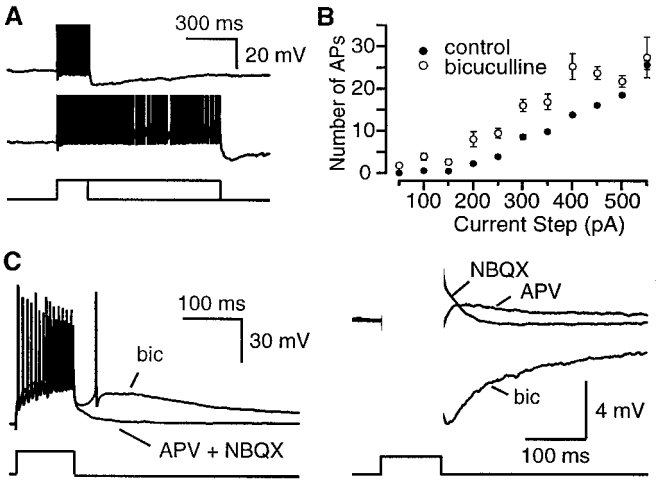

Fig. 4. The effect of recurrent IPSPs on mitral cell firing. (*A*) The amplitude of the *in vitro* recurrent IPSP is unaffected by changing the duration of current step from 200 ms to 1 s. APs are clipped. (*B*) *In vitro*, the number of APs elicited by a 100-ms current step of a given amplitude is shown for control conditions and in the presence of bicuculline (20–40 μM). (*C*) (*Left*) Application of bicuculline *in vitro* resulted in prolonged depolarization and AP firing after termination of current injection. The depolarization was blocked by addition of APV (25 μM) and NBQX (10 μM). (*Right*) Average traces show the bicuculline-, APV-, and NBQX- (or CNQX-) sensitive components of the response obtained by digital subtraction (APs are blanked).

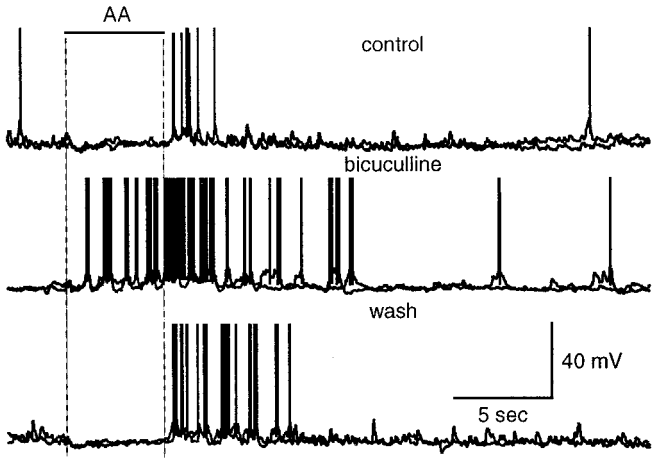

Fig. 5. Odor-evoked lateral inhibition in mitral cells. Presentation of AA under control conditions (*Top*) caused initial hyperpolarization, followed by a transient burst of spikes after termination of the stimulus. This hyperpolarization was blocked reversibly by bicuculline (*Middle* and *Bottom*). Data are two traces superimposed to illustrate the reliability of the odor-evoked responses.

of 0.1 to 5 s and compared the amplitude of the recurrent IPSP evoked as a function of stimulus duration. The amplitude of the recurrent IPSP was unaffected by increasing the duration of the current step while maintaining a constant AP frequency of ≈50 Hz (100 ms with 1-, 2-, 4-, and 5-s pulses; $F_{(4,15)} = 0.07, P = 0.989$, one-way ANOVA; Fig. 4*A*). This observation indicates that the recurrent IPSP is not attenuated by long periods of high frequency firing and maintains its effectiveness during long periods of sensory stimulation (e.g., Fig. 1*B*, cell 2 and Fig. 2*A*).

When the recurrent IPSP was abolished by application of bicuculline (20–40 μM), we found that current steps (100 ms) elicited more APs than in control conditions (e.g., a 200-pA step: 2.3 ± 0.2 APs in control vs. 8.0 ± 1.8 APs in bicuculline; Fig. 4*B*, $n = 8$ cells). In the presence of bicuculline, current-evoked APs were followed by a depolarization (2.1 ± 0.9 mV amplitude at peak evoked by 10 AP; $n = 5$; Fig. 4*C Left*) that in some cases produced AP firing (Fig. 4*C Left*). This prolonged depolarization was blocked by glutamate receptor antagonists (APV, 25 μM and NBQX or CNQX, 10 μM), suggesting that AP-evoked release of glutamate from a mitral cell evokes a recurrent excitatory postsynaptic potential (EPSP) mediated by both *N*-methyl-D-aspartate (NMDA) and α-amino-3-hydroxy-5-methyl-4-isoxazolepropionic acid (AMPA) receptors (32–37; Fig. 4*C Right*). By subtracting the averaged response recorded in the presence of bicuculline from the average control response, we found that the recurrent EPSP *in vitro* reduces the bicuculline-sensitive component by ≈40% (isolated IPSP = −5.7 ± 1.5 mV, isolated EPSP = 2.4 ± 0.9 mV, for 7 APs, $n = 4$ cells; Fig. 4*C Right*). These data show that recurrent inhibition reduces the rate of mitral cell firing and is masked in part by glutamatergic self excitation.

Odor Evoked Lateral Inhibition. The second type of response of mitral cells to odorants (Fig. 1*C*) was characterized by a hyperpolarization during the initial 1–2 s of odor presentation (2, 30, 38–39). This hyperpolarization attenuated with time and often was accompanied by an increase in membrane noise (e.g., Fig. 1*C*, cells 3–5 and Fig. 5 *Top*). Cells that exhibited this initial hyperpolarization during stimulus presentation under control conditions fired APs in response to the same stimulus after superfusion of bicuculline over the surface of the MOB ($n = 3$; Fig. 5 *Middle*). Because the hyperpolarization was not preceded by AP firing, these data show that $GABA_A$ receptor-mediated lateral inhibition prevents odor-evoked firing in mitral cells. Moreover, the attenuation of the hyperpolarization during the odor presentation suggests that the amplitude of lateral inhibition decreases as a function of stimulus duration. Thus, lateral inhibition can prevent or delay firing in mitral cells receiving active ORN input.

Decremental AP Propagation and Ca^{2+} Transients in Lateral Dendrites. Granule cell-mediated dendrodendritic inhibition underlies recurrent and lateral inhibition between mitral cells and depends on $[Ca^{2+}]$-dependent glutamate release from mitral cell lateral dendrites. We measured AP propagation and the AP-evoked increase of $[Ca^{2+}]$ in these dendrites to determine how patterns comparable to odor-evoked mitral cell activity determine the propagation of APs in lateral dendrites and the concomitant transient rise in dendritic $[Ca^{2+}]$. Simultaneous whole-cell voltage recordings from mitral cell somata and lateral dendrites showed that single APs decreased in amplitude by 22% per 100 μm (linear fit to data $R^2 = 0.52$, $n = 13$; Fig. 6 *A* and *B*) as they propagated from the soma into lateral dendrites. In contrast, APs in the apical dendrite did not attenuate with distance (<0.1% increase per 100 μm, $n = 5$; Fig. 6*B*; refs. 22 and 23). Because odors can evoke mitral cell firing at rates higher than 250 AP s^{-1}, we examined whether propagation in lateral dendrites depended on repetitive APs (40). When a train of APs was elicited at the soma, propagation of APs into distal lateral dendrites increased with AP number. For dendritic recordings further than 75 μm from the soma, attenuation was reduced from 41% for the first AP to 31% by the eighth AP ($n = 6$; Fig. 6 *C* and *D*). This improved propagation was associated with both an increase in AP amplitude in the dendrite and a decrease in AP amplitude in the soma. The larger peak depolarization of the later APs in a train may, therefore, result in more effective activation of voltage-dependent calcium channels in the lateral dendrites and thus in increased lateral inhibition.

Because lateral inhibition is driven by Ca^{2+}-dependent glutamate release (17, 19) from the lateral dendrites of mitral cells,

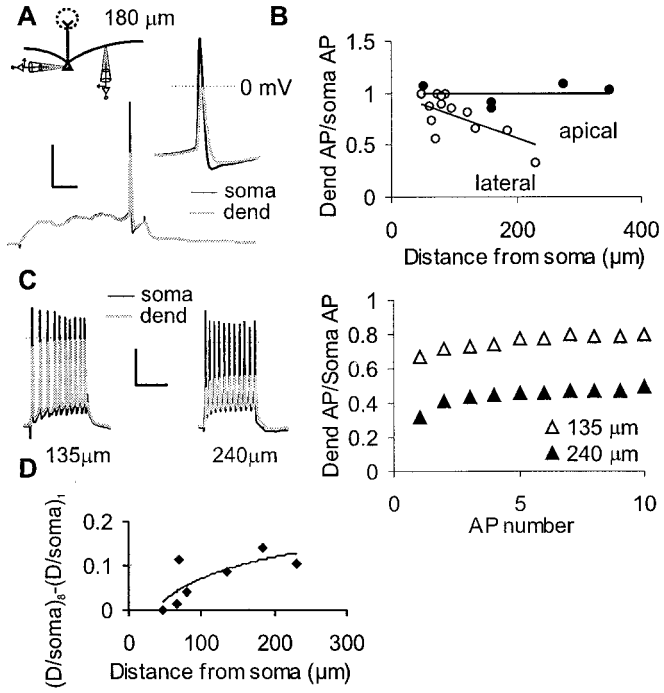

Fig. 6. AP propagation in mitral cell lateral dendrites *in vitro*. (*A*) Simultaneous whole-cell recordings from the soma (black line) and a lateral dendrite (180 μm from the soma, gray line) of a mitral cell show that APs in the lateral dendrite are smaller than those recorded in the soma. [Scale bar indicates 25 mV and 20 ms (5 ms for *Inset*).] (*B*) The summary graph shows the ratio of the dendritic-to-somatic AP amplitude for lateral dendrites (○; $n = 12$) and apical dendrites (●; $n = 5$), plotted as a function of distance from the soma. Lines show the best linear fit. (*C*) Data from a single cell show that the amplitude of somatic APs attenuates throughout a high-frequency train, whereas the amplitude of APs recorded in the lateral dendrite (at two locations) increases. (Scale bar indicates 25 mV and 60 ms.) (*Right*) The ratio of dendritic to somatic AP amplitude in lateral dendrites increases with AP number, and this increase is larger at the distal location. (*D*) Data from seven cells show the difference between the propagation ratios for the eighth and the first AP in a train. This difference increases with the distance from the soma.

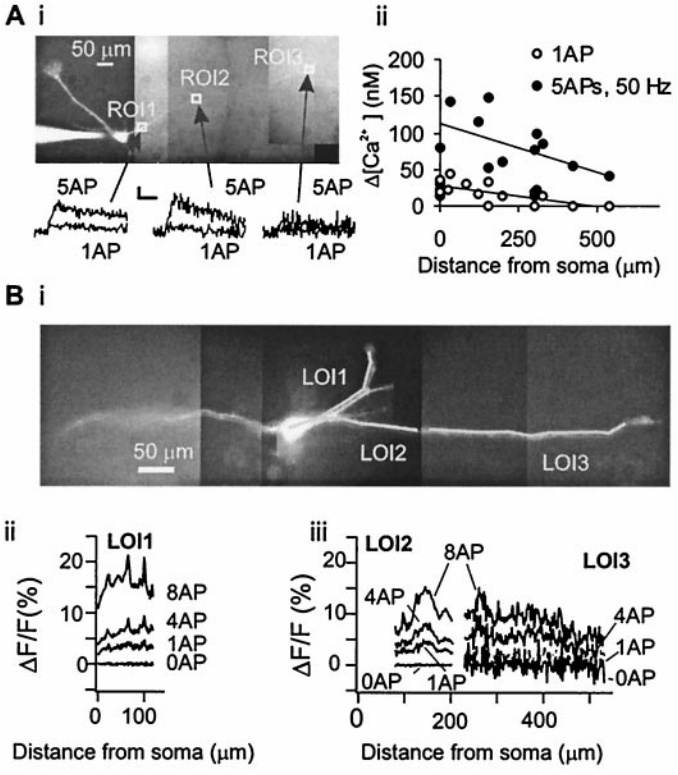

Fig. 7. AP-dependent Ca^{2+} transients in mitral cell dendrites recorded *in vitro*. (*Ai*) Fluorescence image of a mitral cell filled with the calcium indicator Fura-2 (50 μM). (*Upper*) Ca^{2+} transients evoked by one and five APs (at 50 Hz) recorded from indicated regions of interest (ROI) show the attenuation of the Ca^{2+} transient with distance along the lateral dendrite. (Scale bar indicates 20 nM $\Delta[Ca^{2+}]$ and 100 ms.) (*Aii*) Peak $\Delta[Ca^{2+}]$ evoked by one and five APs (at 50 Hz) plotted against the distance along the lateral dendrite at which it was recorded ($n = 19$ ROI from 13 cells). Lines indicate the best linear fit to data. (*Bi*) Fluorescence image of a mitral cell filled with calcium orange (50 μM). Lines of interest (LOI1, LOI2, and LOI3) indicate the regions of the dendrite where fluorescence measurements (in *Bii* and *Biii*) were made. (*Bii* and *Biii*) $\Delta F/F$ measured along LOI1, LOI2, and LOI3 plotted against distance from the soma for the indicated number of APs (0, 1, 4, or 8). Data were collected over an interval of 67–134 ms after the last AP.

we measured the spatial profile of Ca^{2+} transients along these dendrites. Calcium transients observed in response to single somatically evoked APs decreased with distance by 20% per 100 μm from the soma (linear fit to data, $R^2 = 0.47$, $n = 19$; Fig. 7*A*). When multiple APs were evoked, the amplitude of calcium transients increased nonlinearly with AP number. In the distal lateral dendrites (>250 μm from the soma), calcium transients following five APs were 7-fold larger than those evoked by a single AP (1 AP = 16.0 ± 6.8 nM peak $\Delta[Ca^{2+}]$ vs. 5 AP = 115.1 ± 40.8 nM peak $\Delta[Ca^{2+}]$, $n = 7$ cells; Fig. 7*A*). In some cells, single APs evoked no measurable calcium transient in distal regions of the lateral dendrite (>300 μm from the soma), whereas trains of APs evoked large calcium elevations in these same regions (Fig. 7 *Aii* and *Biii*). Thus, repeated APs act cooperatively to elevate $[Ca^{2+}]$ in distal segments of lateral dendrites (Fig. 7 *A* and *B*). This observation suggests that, although single APs will fail to evoke glutamate release from the distal half of a lateral dendrite, repetitive APs will progressively recruit release from more distal release sites.

Calcium transients in lateral dendrites evoked by multiple APs increased substantially in the presence of bicuculline ($\Delta F/F$ evoked by 5 APs at 50 s^{-1} was 22 ± 6% in controls vs. 39 ± 8% with bicuculline, $n = 5$) in dendritic segments >300 μm from the soma. Single AP-evoked calcium transients were unaffected by the addition of bicuculline ($\Delta F/F$ evoked by 1 AP was: 3.2 ± 0.4% vs. 3.7 ± 0.6%) in these same dendritic segments. These data suggest that recurrent inhibition regulates the spatial extent of AP propagation evoked by repeated AP firing in mitral cells.

Discussion

Here we describe two general patterns of odor-evoked AP firing in mitral cells of the mammalian MOB and detail cellular mechanisms that may give rise to these two patterns. Strongly activated mitral cells decrease their firing rates during odor presentation. In other mitral cells, odor-evoked inhibition delays or prevents firing, even though these cells receive active olfactory nerve input. Both these effects are mediated by $GABA_A$ receptors.

Recurrent inhibition is the most likely mechanism underlying the decrease in firing rate during stimulus presentation seen in strongly activated mitral cells. Although ORNs have been shown to desensitize in response to odor presentations, in the presence of bicuculline, mitral cells fire at almost constant rates for the duration of the stimulus. This response indicates that desensitization of ORNs is unlikely to contribute to the observed accommodation of AP firing rates in mitral cells.

Odor-evoked hyperpolarizations of mitral cells are blocked by bicuculline, indicating that they represent lateral inhibition

mediated by activation of granule and/or periglomerular cells (8, 9), rather than an odor-evoked decrease in tonic ORN firing rates (1, 2) or a $GABA_B$ receptor-mediated decrease in glutamate release from ORN terminals (38, 39, 41). The data suggest that lateral inhibition controls the latency between sensory input and onset of mitral cell activity.

Both recurrent and lateral inhibition are likely to depend on depolarization-evoked Ca^{2+} influx into mitral cell lateral dendrites. Although APs in the apical dendrite of mitral cells propagate reliably and fully for the length of the dendrite (22, 23), APs in the lateral dendrites do not. This difference in AP propagation in different dendrites of the same neuron may be unique to mitral cells and may reflect the distinct and specialized functions of apical vs. lateral dendrites. The amplitude of $[Ca^{2+}]$ transients in distal lateral dendrites increases steeply with AP number, suggesting that repetitive mitral cell firing will be much more effective in causing glutamate release and excitation of granule cells. Thus, an increase in AP frequency will result in more widespread release of glutamate from lateral dendrites and in a larger spatial extent of lateral inhibition across the MOB. We propose that, at least in part, activity-dependent AP propagation, along with the resultant $[Ca^{2+}]$ increase in mitral cell lateral dendrites, controls the amount of lateral and recurrent inhibition received by an individual mitral cell.

Mitral cells receiving relatively strong ORN input fire relatively earlier than those with weaker input. As their AP frequency decreases with time because of recurrent inhibition, the extent of AP propagation into lateral dendrites is reduced. This decrease results in a gradual reduction in activation of granule cells receiving input from distal regions of the lateral dendrites. The lateral inhibition evoked by these granule cells is then attenuated, allowing mitral cells to fire during the later phases of odor stimulation. Therefore, a mitral cell's recurrent inhibition shapes not only its own temporal AP pattern but also the response onset of other mitral cells. This view predicts that, by means of activity-dependent dendrodendritic inhibition, mitral cells compete for "excitation space" across the bulb to represent a spatiotemporal olfactory code (4, 42–45). The structure of this putative excitation space would be governed largely by the geometry of the lateral dendrites of mitral cells and the activity-dependent decremental-AP propagation into these dendrites.

We thank Julius Zhu for early technical advice and Michael Brecht, Matthew Larkum, Carl Petersen, Rainer Friedrich, Andreas Schaefer, and Gordon Shepherd for comments on earlier versions of the manuscript. This work was supported by fellowships from the Alexander von Humboldt Foundation (to T.M. and N.U.) and the National Health and Medical Research Council of Australia (to T.M.). T.M. carried out *in vivo* experiments, whereas N.U. carried out all *in vitro* experiments.

1. Duchamp-Viret, P., Chaput, M. A. & Duchamp, A. (1999) *Science* **284,** 2171–2174.
2. Duchamp-Viret, P., Duchamp, A. & Chaput, M. A. (2000) *J. Neurosci.* **20,** 2383–2390.
3. Kauer, J. S. (1991) *Trends Neurosci.* **14,** 79–85.
4. Laurent, G. (1999) *Science* **286,** 723–728.
5. Rall, W., Shepherd, G. M., Reese, T. S. & Brightman, M. W. (1966) *Exp. Neurol.* **14,** 44–56.
6. Woolf, T. B., Shepherd, G. M. & Greer, C. A. (1991) *Synapse* **7,** 181–192.
7. Price, J. L. & Powell, T. P. S. (1970) *J. Cell Sci.* **7,** 125–155.
8. Nicoll, R. A. (1971) *Brain Res.* **35,** 137–149.
9. McLennan, H. (1971) *Brain Res.* **29,** 177–187.
10. Jahr, C. E. & Nicoll, R. A. (1980) *Science* **207,** 1473–1475.
11. Jahr, C. E. & Nicoll, R. A. (1982) *J. Physiol. (London)* **326,** 213–234.
12. Yokoi, M., Mori, K. & Nakanishi, S. (1995) *Proc. Natl. Acad. Sci. USA* **92,** 3371–3375.
13. Shepherd, G. M. & Greer, C. A. (1998) in *Olfactory Bulb*, ed. Shepherd, G. M. (Oxford Univ. Press, New York), pp. 159–203.
14. Segev, I. (1999) *Nat. Neurosci.* **2,** 1041–1043.
15. Yamamoto, C., Yamamoto, T. & Iwama, K. (1963) *J. Neurophysiol.* **26,** 403–415.
16. Mori, K. & Takagi, S. F. (1978) *J. Physiol. (London)* **279,** 589–604.
17. Isaacson, J. S. & Strowbridge, B. W. (1998) *Neuron* **20,** 749–761.
18. Schoppa, N. E., Kinzie, J. M., Sahara, Y., Segerson, T. P. & Westbrook, G. L. (1998) *J. Neurosci.* **18,** 6790–6802.
19. Chen, W. R., Ziong, W. & Shepherd, G. M. (2000) *Neuron* **25,** 625–633.
20. Halabisky, B., Friedman, D., Radojicic, M. & Strowbridge, B. W. (2000) *J. Neurosci.* **20,** 5124–5134.
21. Orona, E., Rainer, E. C. & Scott, J. W. (1984) *J. Comp. Neurol.* **226,** 346–356.
22. Chen, W. R., Midtgaard, J. & Shepherd, G. M. (1997) *Science* **278,** 463–467.
23. Bischofberger, J. & Jonas, P. (1997) *J. Physiol. (London)* **504,** 359–365.
24. Kauer, J. S. & Firestein, S. J. (1995) in *Methods for Air-Borne and Aqueous Stimulus Delivery in Olfactory Research*, eds. Spielman, A. I. & Brand, J. G. (CRC, Boca Raton, FL).
25. Horikawa, K. & Armstrong, W. E. (1988) *J. Neurosci. Methods* **25,** 1–11.
26. Stuart, G. J., Dodt, H.-U. & Sakmann, B. (1993) *Pflügers Arch.* **423,** 511–518.
27. Blanton, M. G., Lo Turco, J. J. & Kriegstein, A. R. (1989) *J. Neurosci. Methods* **30,** 203–210.
28. Grynkiweicz, G., Poenie, M. & Tsien, R. Y. (1985) *J. Biol. Chem.* **260,** 3440–3450.
29. Helmchen, F., Imoto, K. & Sakmann, B. (1996) *Biophys. J.* **70,** 1069–1081.
30. Kauer, J. S. (1974) *J. Physiol. (London)* **243,** 695–715.
31. Jahr, C. E. & Nicoll, R. A. (1982) *Nature (London)* **297,** 227–229.
32. Nicoll, R. A. & Jahr, C. E. (1982) *Nature (London)* **296,** 441–444.
33. Isaacson, J. S. (1999) *Neuron* **23,** 377–384.
34. Aroniadou-Anderjaska, V., Ennis, M. & Shipley, M. T. (1999) *J. Neurophysiol.* **81,** 15–28.
35. Carlson, G. C., Shipley, M. T. & Keller, A. (2000) *J. Neurosci.* **20,** 2011–2021.
36. Nowycky, M. C., Mori, K. & Shepherd, G. M. (1981) *J. Neurophysiol.* **46,** 649–658.
37. Friedman, D. & Strowbridge, B. W. (2000) *J. Neurophysiol.* **84,** 39–50.
38. Nickell, W. T., Behbehani, M. M. & Shipley, M. T. (1994) *Brain Res. Bull.* **35,** 119–123.
39. Wachowiak, M. & Cohen, L. B. (1999) *J. Neurosci.* **19,** 8808–8817.
40. Spruston, N., Schiller, Y., Stuart, G. & Sakmann, B. (1995) *Science* **268,** 297–300.
41. Aroniadou-Anderjaska, V., Zhou, F.-M., Priest, C. A., Ennis, M. & Shipley, M. T. (2000) *J. Neurophysiol.* **84,** 1194–1203.
42. Adrian, E. D. (1942) *J. Physiol. (London)* **100,** 459–473.
43. Freeman, W. J. (1983) *Biol. Psychiatry* **18,** 1107–1125.
44. Ottoson, D. (1959) *Acta Physiol. Scand.* **47,** 136–148.
45. Hopfield, J. J. (1995) *Nature (London)* **376,** 33–36.